Journal of Catalysis 271 (2010) 104–114

Contents lists available at ScienceDirect

Journal of Catalysis

journal homepage: www.elsevier.com/locate/jcat

Weakly bound capping agents on gold nanoparticles in catalysis: Surface poison?

A. Quintanilla [a,*], V.C.L. Butselaar-Orthlieb [b], C. Kwakernaak [c], W.G. Sloof [c], M.T. Kreutzer [d], F. Kapteijn [b]

[a] Chemical Engineering Section, Facultad de Ciencias, Universidad Autónoma de Madrid, Campus de Cantoblanco, 28049 Madrid, Spain
[b] Catalysis Engineering, DelftChemTech, Delft University of Technology, Julianalaan 136, 2628 BL Delft, The Netherlands
[c] Department of Materials Science, Faculty of 3mE, Delft University of Technology, Julianalaan 136, 2628 BL Delft, The Netherlands
[d] Process and Product Engineering, DelftChemTech, Delft University of Technology, Julianalaan 136, 2628 BL Delft, The Netherlands

ARTICLE INFO

Article history:
Received 16 December 2009
Revised 8 February 2010
Accepted 9 February 2010
Available online 15 March 2010

Keywords:
Gold
Capping agent
Metallic colloid
Selective oxidation
Benzyl alcohol
Surface poison
Selectivity
Liquid phase
Particle size effect
XPS

ABSTRACT

The influence of the concentration and nature of weakly bound capping agents on the catalytic activity and selectivity of gold nanoparticles is explored in the selective liquid phase oxidation of benzyl alcohol with oxygen and complemented with a detailed XPS analysis. Two nitrogen-based capping agents, dodecylamine (DDA) and poly(vinyl-pyrrolidone) (PVP) and different gold catalysts (supported and unsupported gold nanoparticles, a reference gold catalyst with and without exposure to capping agents) have been used. The colloid nanoparticle-based catalyst exhibits a high activity at mild conditions (TOF = $\sim 10^4\ h^{-1}$ at 353 K in air). The interaction of alumina support–nanoparticle induces the presence of cationic gold and more surface gold atoms and, hence, catalytic activity although capping agent is still present. The activity is the highest for the largest gold particles (~6.4 nm), correlating with sites in larger surface planes.

Weakly bound capping agents lower the accessibility to the active sites and may act as catalyst surface poison. Selecting the appropriate capping agent for the nanoparticles synthesis (weakly adsorbing on the particle and promoting polycrystallinity), nanoparticles with twinning defects and enhanced catalyst activity are produced, compensating the negative effect of diffusional hindrance. On the other hand, the selectivity to benzaldehyde at higher conversions is dominated by gold particle size, increasing with decreasing size, and independent of the presence of capping agents and twinning defects.

1. Introduction

Capping agents, protective agents or stabilizers are molecules (*i.e.* dendrimers, polymers and surfactants) employed in the preparation of metallic nanocrystals by wet chemistry [1–4]. Their functions are to avoid the aggregation of the nanoparticles in solution and to control the size and shape at the crystallographic level (growth is limited at the crystal plane where the capping agent is binding and promoted at the crystal plane where binding is weak) [5–9]. When these metallic nanocrystals are used as high-tech catalysts, the major challenge is to obtain "clean" nanoparticles before or after their deposition on a support without altering the precise nanoparticle structure responsible for their catalytic function.

An elegant method for the removal of the excess of the capping agent, which clearly affects the catalytic action of the particles in gas–solid [10–14] and liquid–gas–solid reactions [15–19], consists of the introduction of a large excess of a solvent in the colloidal suspension such as acetone or methanol that provokes the extraction of the capping agent and the flocculation of the nanoparticles. Then, precipitated nanoparticles are separated and re-dispersed in a selected solvent [20–24]. However, capping agents still remain adsorbed on the nanoparticles, usually in low concentration, depending on the affinity between the metal and the functional group of the capping agent [22,23]. Therefore, capping agents could still compete with reactants and products for the adsorption sites or hamper their accessibility, thereby altering the catalytic action of the particle. As an example, the activity of gold catalysts is detrimentally affected when (strong) covalent binding capping agents (*i.e.* alkanethiol molecules and phosphine complexes) are present in minute amounts [12,13,25]. Furthermore, the capping agent–support affinity is an additional parameter to be considered. The capping agent can affect the particle location on the support modifying the gold shielding caused by the support which will have consequences on the reactivity, as studied with gold-on-carbon catalysts and two different capping agents, *N*-dodecil-*N*,*N*-dimethyl-3-amino-1-propan sulphonate and polyvinyl alcohol [18].

Herein, we analyse the influence of the concentration and nature of weakly bound capping agents on the catalytic activity and selectivity of gold nanoparticles used in a selective oxidation reaction, *viz.* the oxidation of benzyl alcohol. Catalytic data are complemented with a thorough TEM and XPS analyses. The selected capping agents are dodecylamine (DDA), a novel surfactant [26], and poly(vinyl-pyrrolidone) (PVP), a commonly used polymer in the preparation of metallic nanoparticles [27–31]. The choice for these nitrogen-based capping agents was made to enable eventual

* Corresponding author. Fax: +34 914973516.
E-mail address: asun.quintanilla@uam.es (A. Quintanilla).

0021-9517/$ - see front matter © 2010 Elsevier Inc. All rights reserved.
doi:10.1016/j.jcat.2010.02.013

complete oxidative removal, unlike sulphur- or phosphorous-based capping agents. The latter bind stronger and may produce smaller particles but leave undesired residues on the catalyst after oxidation. The effect of the used capping agents is compared in three ways, by using supported and unsupported gold nanoparticles, using bare supported gold particles in a reference catalyst and using the latter after exposure to capping agents. In the latter approach, we study the effect of the presence of residual amounts of a weakly bound capping agent on particles of exactly the same size, morphology and crystalline structure. Also, their effect on the performance of a reference gold catalyst is evaluated.

2. Experimental

2.1. Catalyst preparation

2.1.1. Preparation of gold colloids

Metallic gold nanoparticles with dodecylamine (DDA) were prepared following the methodology described by Chen and Wang [26] which is based on a novel water–cyclohexane two-phase system at room conditions. In 25 mL of cyclohexane, 0.75 g of DDA (Sigma–Aldrich) was dissolved (J.T. Baker), then 6 mL aqueous formaldehyde (37 wt.% in water, Sigma–Aldrich) was added and DDA could react with formaldehyde to yield the reductive intermediate, dodecylaminomethanol (DDAM):

$$CH_3(CH_2)_{10}CH_2NH_2 + HCHO \rightarrow CH_3(CH_2)_{10}CH_2NHCH_2OH \quad (1)$$

After vigorously stirring for 10 min at 298 K, the cyclohexane phase containing the reductive intermediate was separated out. Ten millilitre aqueous 4 g/L $HAuCl_4$ (Sigma–Aldrich) solution was added into the separated cyclohexane solution under vigorous stirring, and the amine–methanol group $-NHCH_2OH$ is oxidized to $-NHCOOH$ by Au^{3+} which is as the same time reduced to Au^0. The $-NHCOOH$ group is not stable and decomposes into $-NH_2$ and formic acid. Thus, DDA is released and adsorbs and assembles on the nanoparticle surface. At this moment, the colour of the organic phase turned deep ruby red:

$$CH_3(CH_2)_{10}CH_2NHCH_2OH + Au^{3+} \xrightarrow{O2} CH_3(CH_2)_{10}CH_2NH_2 - Au^0 + HCOOH + H_2O \quad (2)$$

Metallic gold nanoparticles with poly(vinyl-pyrrolidone) (PVP) were prepared following a methodology similar to that described by Domínguez-Domínguez et al. [21] which involves the reduction of 24 mg of $HAuCl_4$ by 120 mL anhydrous ethylene glycol (Sigma–Aldrich) in the presence of PVP (PVP40T, Sigma–Aldrich) at 353 K for 3 h:

$$HO - CH_2 - CH_2 - OH \xrightarrow{T} CH_3 - CHO + H_2O \quad (3)$$

$$6(CH_3 - CHO) + 2(HAuCl_4) \xrightarrow{T} 3(CH_3 - CO - CO - CH_3) + 2Au^0 + 8HCl \quad (4)$$

The solution had also a deep red colour.

The operating conditions for the preparation of both gold colloid solutions are summarized in Table 1.

2.1.2. Preparation of solid catalysts

The reference catalyst 0.8%Au/Al_2O_3 (2.5-nm gold particle size, BC17) supplied by World Gold Council (WGC), with the gold nanoparticles already in immobilized form after their preparation by deposition–precipitation, was coated with DDA and PVP (indicated by WGC-DDA and WGC-PVP catalysts, respectively) by the following procedure: 2 g of WGC catalyst (d_p = 50–70 μm) was stirred overnight with the corresponding capping agent solution, 0.75 g of DDA in 25 mL of toluene, for WGC-DDA, and 0.75 g of PVP in 25 mL of distilled water, for WGC-PVP. After coating, catalysts were filtered and washed with acetone and then ethanol under vigorous stirring for 1 h.

Other batches of catalyst were prepared by immobilization of the preformed gold nanoparticles on commercial γ-Al_2O_3 (Akzo Chemie, ref. 31814) by adsorption. The appropriate volume of (i) the 'as-prepared' colloid (CAT-DDA) or (ii) the colloid after first washing the excess of capping agents with acetone and subsequent re-dispersion of the nanoparticles in cyclohexane (CAT-DDA (w)) or water (CAT-PVP (w)) was stirred overnight with the corresponding mass of γ-Al_2O_3 (d_p = 50–70 μm) in order to prepare the 1% wt. Au/Al_2O_3 catalysts. The red colour of the colloid solution faded overnight. The resulting catalysts had a pink colour, more intense for the DDA-coated nanoparticles. Subsequently, the catalysts were filtered and dried at room temperature under a flow of 100 mL(STP)/min N_2 for 24 h.

After reaction, the catalyst was separated from the reaction mixture by centrifugation and regenerated by washing with distilled water for 1 h. The regenerated catalyst is filtered and reused in a next run, not always under the same conditions.

2.2. Catalyst characterization

The gold particle size distribution was obtained from TEM (Philips CM30UT) analysis, by counting at least 500 particles. The bulk content of gold was measured by a graphite furnace AAS (Perkin–Elmer 4100ZL).

The XPS measurements were performed with a PHI 5400 ESCA provided with a dual Mg/Mg anode X-ray source, a hemispherical capacitor analyser and a 5 keV Ar^+ ion-gun. The electron input lens to the analyser was set at a take-off angle of 45° with respect to the sample surface normal. The aperture of the electron input lens was such that an area of 3.5 × 1.4 mm was analysed. All spectra were recorded using non-monochromatic Mg Kα (1253.6 eV) radiation. The energy scale of the electron analyser was calibrated with a standard procedure [32] implying that Au^0 appears at 84.00 eV. The X-ray source was operated at an acceleration voltage of 13 kV and power of 200 W in all instances. During the spectrum acquisition, the background pressure of the ultra-high vacuum system was 5×10^{-8} mbar or better. The spectra of the C *1s*, N *1s*, O *1s* and combined Al *2p* – Au *4f* photoelectron regions were recorded with a pass energy of 35.75 eV and a step size of 0.2 eV, see Table 2. Usually, the presence of adventitious or aliphatic carbon on samples investigated using XPS provides a ready to use and stable reference to correct for static charging of the sample [33]. Then, the C *1s* line is set at 284.8 eV and 285.0 eV for adventitious and aliphatic carbon, respectively. However, the complex structure of C *1s* spectra measured of the catalysts studied here rendered the C *1s* line

Table 1
Summary of the experimental conditions for the preparation of gold colloid solutions.

Precursor	Reducing agent	Capping agent	Reducing agent/Au (mol)	Capping agent/Au (mol)	C_{Au} (mM)	T (K)	t (h)
$HAuCl_4$	DDAM	DDA	34.5	34.5	3.4	298	1
$HAuCl_4$	EG[a]	PVP	18×10^3	10	0.6	353	3

[a] EG is also the solvent.

Table 2
Acquisition region and area sensitivity factors for the photoelectron lines analysed.

Spectral lines of C	Region (eV)	Acquisition time per point (s)	Sensitivity factor
C *1s*	280–300	25	0.314
N *1s*	395–415	25	0.499
O *1s*	520–550	10	0.677
Al *2p*	65–100	30	0.254
Au *4f*	65–100	30	6.805

not suitable for static charge correction, due to the presence of other carbonaceous species than adventitious or aliphatic carbon. Therefore, in this work, the alumina support is taken as a reference. As an average value for Al *2p*, a binding energy of 74.3 ± 0.2 eV was adopted implying 531.3 ± 0.2 eV for O *1s* [34]. The spectra were evaluated with Multipak 8.0 software (Physical Electronics). The photoelectron spectra recorded were corrected for the satellites generated due to the non-monochromatic character of the Mg Ka X-ray source. Further, the static charge correction was applied (see above). A Shirley-type background was then subtracted from the spectra. Next, the area of the photoelectron spectral lines was determined and using the sensitivity factor presented in Table 2 [35], the atomic fraction of the elements present at the surface (C, O, Al, N, Au) was determined. The deconvolution of the Au *4f* photoelectrons was performed with the following: (i) a full width half maximum (FWHM) of 1.12 eV as obtained from pure metal gold with pseudo-Voigt functions possessing 40% Gaussian character, (ii) the $4f_{7/2}$ and $4f_{5/2}$ doublet separation of 3.66 eV and (iii) using an area ratio of 0.75 for the $4f_{5/2}$ peak relative to the $4f_{7/2}$ peak.

The efficiency of the removal of capping agent was determined by TG Analysis (TGA/SDTA851^e thermobalance, Mettler-Toledo), heating the sample in air from 298 to 1173 K at 10 K/min.

2.3. Selective oxidation

The reactions were performed in 20 mL of toluene (Merck) with K_2CO_3 (Alfa Aesar) (K_2CO_3:BOL = 1:1 mol). Benzyl alcohol (5.5 mmol) (Sigma–Aldrich) and 0.2 g of catalysts (BOL:Au = 550–679 mol, for a gold loading of 0.8–1 wt.%) were charged to the reactor, a magnetically stirred three-necked flask with a reflux. The mixture was then heated to 353 K at atmospheric pressure. When this temperature was reached, an air flow of 100 mL(STP)/min bubbled through the mixture and the stirring at 1200 rpm started. The reaction hardly proceeds in the absence of catalyst (6% conversion of benzyl alcohol and total selectivity to benzaldehyde were achieved after 1.5 h of reaction). A previous work confirmed that no conversion of benzyl alcohol occurred over the alumina alone [36]. In addition, some experiments were performed at a lower stirring rate (1000 rpm) to confirm the absence of external mass transfer limitations. The γ-Al_2O_3 particle size employed (d_p = 50–70 μm) also assures the absence of internal mass limitations (Wheeler–Weisz modulus <0.15, based on the observed initial rate of the CAT-PVP (w)catalyst).

Liquid samples (100 μL) were collected at different reaction times during 1.5 h and analysed with a Chrompack gas chromatograph (CP9001 autosampler), equipped with a CP Sil 8 CB column (50 m × 0.25 mm), under the following conditions: FID temperature, 523 K; injector temperature, 523 K; and column temperature ramped uniformly from 423 to 523 K at 6.7 K/min. The identified intermediates were benzaldehyde and benzoic acid which are obtained according to the following consecutive reaction Scheme 1.

3. Results

3.1. Catalyst characterization

Figs. 1 and 2 show TEM micrographs and particle size distribution of the prepared colloids. The resulting DDA-capped gold nanoparticles are spherical and monocrystalline with the particle size centring at 3.9 ± 0.5 nm (Fig. 1). The PVP-capped gold nanoparticles are also spherical though the larger particles can show facets and steps/edges due to polycrystallinity (Fig. 2). In contrast to DDA-capped gold nanoparticles, the PVP-capped particles are larger (4.8 ± 1.7 nm), polydisperse and polycrystalline. Once immobilized on commercial γ-Al_2O_3, the particle size and distribution increase only when PVP is the capping agent (4.4 ± 0.6, 4.0 ± 0.9 and 6.4 ± 3.2 nm for CAT-DDA, CAT-DDA (w) and CAT-PVP (w), respectively) (Fig. 3).

The gold content measured by AAS and the amount of the capping agent measured as the percentage weight loss by TGA for all the samples are summarized in Table 3. The content of gold in all supported catalysts is around the targeted 1 wt.%. The percentage weight loss is similar for both classes of catalysts, *i.e.* those prepared by coating of the reference catalyst (WGC-DDA and WGC-PVP) and those prepared by immobilization of the presynthesized coated and washed nanoparticles (CAT-DDA (w) and CAT-PVP (w)). Only for CAT-DDA, prepared with the non-washed nanoparticles, an excess of DDA is clearly also adsorbed on the alumina (see differential thermogravimetric and SDTA profiles in Supplementary material).

The gold speciation and elemental composition in atom per cent (at.%) present at the surface of the investigated catalysts, as follows from the XPS analyses, are also reported in Table 3.

The Au $4f_{7/2}$ region is deconvoluted with three curves as shown in Fig. 4 (see, for references on BE values assignment, Section 4 and Refs. [34,45,53,54]). The left and central curves are identified as the neutral atoms of the gold nanoparticles with Au $4f_{7/2}(1)$ associated with the surface atoms and Au $4f_{7/2}(2)$ with the interior atoms; see Table 4. The right curve of Au $4f_{7/2}(3)$ is assigned to monovalent cationic gold, *i.e.* Au^+. The binding energy of this cationic gold line is 1.0 eV higher than that of the neutral gold species corresponding to the central curve. The binding energies derived are presented in Table 4 for all CAT-DDA and the CAT-PVP (w) catalysts. The deconvolution of the WGC specimens were left out because the intensity of the Au *4f* region of the WGC samples was too small to obtain an accurate result (see Supplementary material).

All catalysts contain Au^0 and Au^+ species. The coating of gold with capping agents in the WGC catalyst does not change the

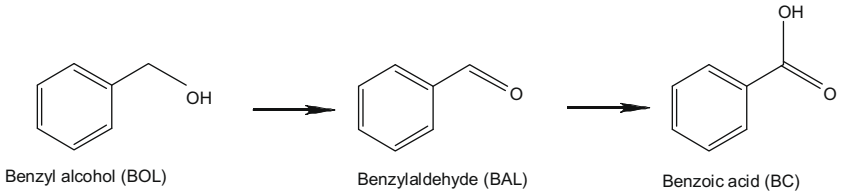

Scheme 1. Reaction pathway in the oxidation of benzyl alcohol with Au/Al_2O_3 catalysts.

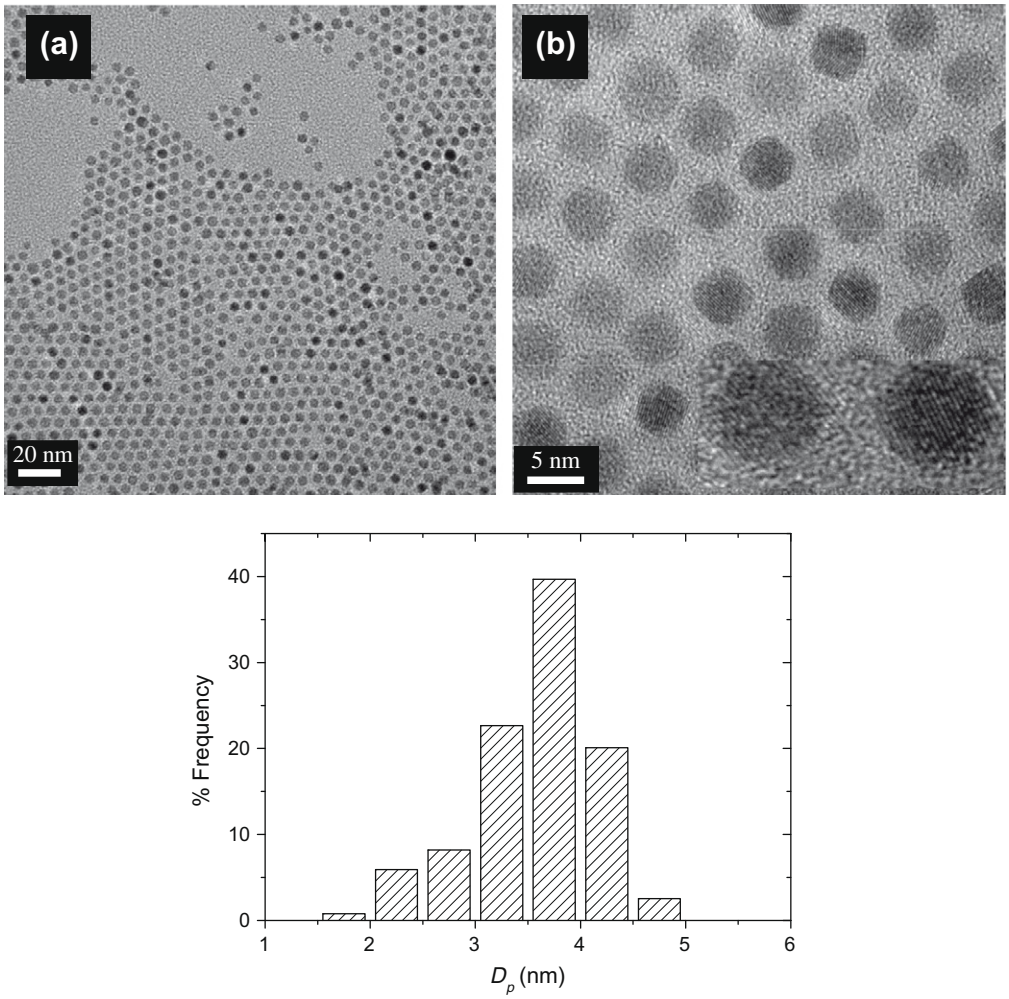

Fig. 1. TEM micrographs (a,b) and particle size distribution histogram corresponding to the colloid prepared with DDA as capping agent. The inset of (b) shows the monocrystallinity of the particles.

Au^+ surface concentration. The amount of nitrogen measured is less for PVP than for DDA-capped nanoparticles (*cf.* WGC-DDA and WGC-PVP in Table 3). PVP is introduced to the system in polymer chains of about 400 monomers whereas DDA is admitted per molecule. It is therefore conceivable that the coverage of the gold nanoparticles with DDA is more effective than the coverage with the long chains of PVP. The lower affinity of PVP for gold is in line with the larger gold particle size in CAT-PVP (w) than in CAT-DDA and CAT-DDA (w).

3.2. Activity and selectivity

Experimentally it is verified that the 'as-prepared' DDA-capped gold sol (3.9 ± 0.5 nm) is not catalytically active for the oxidation of benzyl alcohol at a substrate/gold ratio of 679 (2.4 mL colloid was diluted in 20 mL of reaction media). Once immobilized on the alumina, the sol is slightly active (CAT-DDA catalyst). The results obtained by all the solid catalysts are summarized in Figs. 5–7. High Turn-Over Frequencies, TOFs, (mol benzyl alcohol/mol surface gold/h), up to 10^4 h^{-1}, and selectivities to benzaldehyde (mol benzaldehyde formed per converted mol benzyl alcohol) between 75% and 90% were obtained at a benzyl alcohol conversion of 80% (Fig. 5). Fig. 6 shows the benzyl alcohol conversion-time profiles for the 'as-received' WGC catalyst (0.8 wt.% Au/Al_2O_3) and coated-WGC catalyst exposed to capping agents DDA and PVP. Fig. 7 shows the overall selectivity to benzaldehyde as a function of benzyl alcohol conversion.

The coating of gold with capping agents in the WGC catalyst considerably decreases the TOF values (Fig. 5); a reduction by 70% is observed when a capping agent is present (see the WGC-DDA and WGC-PVP catalysts after the second use, when the excess of capping agent has been removed from the surface). Gradual desorption of the capping agent into the reaction mixture (percentage of nitrogen decreases after the first use of the capped catalysts, Table 3) yields an increase in the activity during the first run, resulting in the S-shaped conversion-time profile (Fig. 6). We refer to trace amounts of both capping agents, since their presence in the solution was not detected by GC.

CAT-DDA catalyst clearly confirms the detrimental effect on the activity by the presence of the capping agent. The initial TOF value increases from 200 h^{-1}, in the fresh CAT-DDA catalyst, to 8500 h^{-1} in the regenerated one. The desorption of DDA from the catalyst surface into the reaction mixture during reaction accounts for this activity increase. DDA in solution could be detected by GC only for the reaction with fresh CAT-DDA that still contained an excess of DDA.

CAT-PVP (w) catalyst has the highest TOF value (Fig. 5), even higher than the WGC catalyst without any capping agent, and in spite of having the largest particle size and a slightly lower concentration of Au^+ species (Table 3).

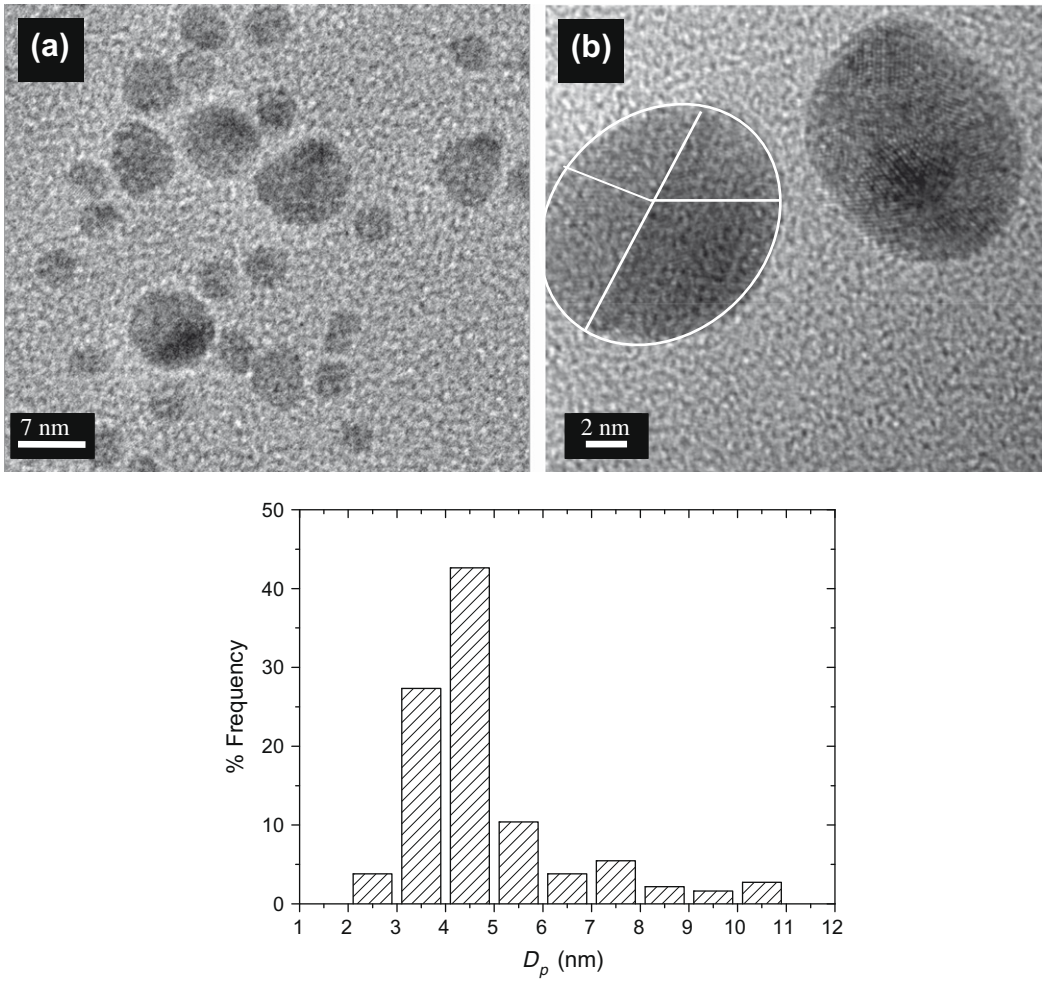

Fig. 2. TEM micrographs (a,b) and particle size distribution histogram corresponding to the colloid prepared with PVP as capping agent. The white lines of (b) indicate the boundaries of the different particle facets, showing the polycrystallinity of the particle.

With regard to selectivity, complete selectivity is achieved at low benzyl alcohol conversions of around 20%, after which it gradually decreases (Fig. 7). CAT-PVP (w) catalyst shows the lowest selectivity whereas WGC the highest (Figs. 5 and 7). The selectivity increases with decreasing gold particle size independent of the presence of a capping agent, namely WGC, WGC-DDA and WGC-PVP catalysts with the same particle size show the same selectivity at equal conversion.

4. Discussion

DDA shows more affinity for gold than PVP. DDA forms a self-assembled layer on the gold particle by a weak covalent bond between the amine group and gold [37]. On the other hand, PVP is a cross-linked polymer wound around the gold particle, and the existence of steric hindrance results in a gold core-porous PVP shell architecture with a coordination of the nitrogen atom and (predominantly) the carbonyl group of the pyrrolidone ring with the particle [38,39]. A schematic illustration with the different configurations is shown in Fig. 8. This difference in assembling around the gold particle probably results in the smaller and better defined particle size for the DDA sample than for PVP. It is worth noting the inactivity of the DDA-capped gold sol. Taking into account the work of Comotti et al. [40], in which 'naked' gold particles are revealed as highly active catalysts in the aerobic oxidation of glucose, it is sensible to consider that the presence of DDA interferes in the gold activity. Due to the excess of DDA reagent used in the preparation of the colloid (DDA/gold molar ratio is one hundred times higher than that expected for the maximum coverage of the gold nanoparticle with DDA, calculations done with d_{NH_2} in DDA = 0.32 nm and $d_{Au\ particle}$ = 3.9 nm), we can confirm that DDA molecules are not only attached to the gold nanoparticles but also dissolved in the reaction media. The molecules shielding the gold nanoparticle (Fig. 8) can occupy the active sites or interfere in their accessibility [41] and DDA in solution can act as a poison, selectively blocking the active sites, as occurs when thiol-based surfactants are introduced along with benzyl alcohol in the reaction media [25]. Likely, by using lower DDA/gold ratios in the colloid preparation, some activity could be expected as observed with PVA-capped gold sols in the oxidation of ethylene glycol [42] and 1,2-diols [41]. In these works, an optimum PVA/gold ratio (around 0.3 wt./wt.) is obtained (in contrast to the 32 wt./wt. used in this work). It was suggested that the values out of the optimum lead to deactivation of the gold sol due to the presence of the capping agent (ratio > 0.3) or to the aggregation of the nanoparticles (ratio < 0.3). Furthermore, it is striking that the activity of the catalyst samples prepared from the washed nanoparticles is equal to that of the bare reference WGC catalyst with smaller gold particles, and at least a factor 10 higher than reported for this reaction at 373 K in pure oxygen [43]. To relate the high activities with the characteristics of the gold particles on the alumina, first the XPS results are thoroughly analysed.

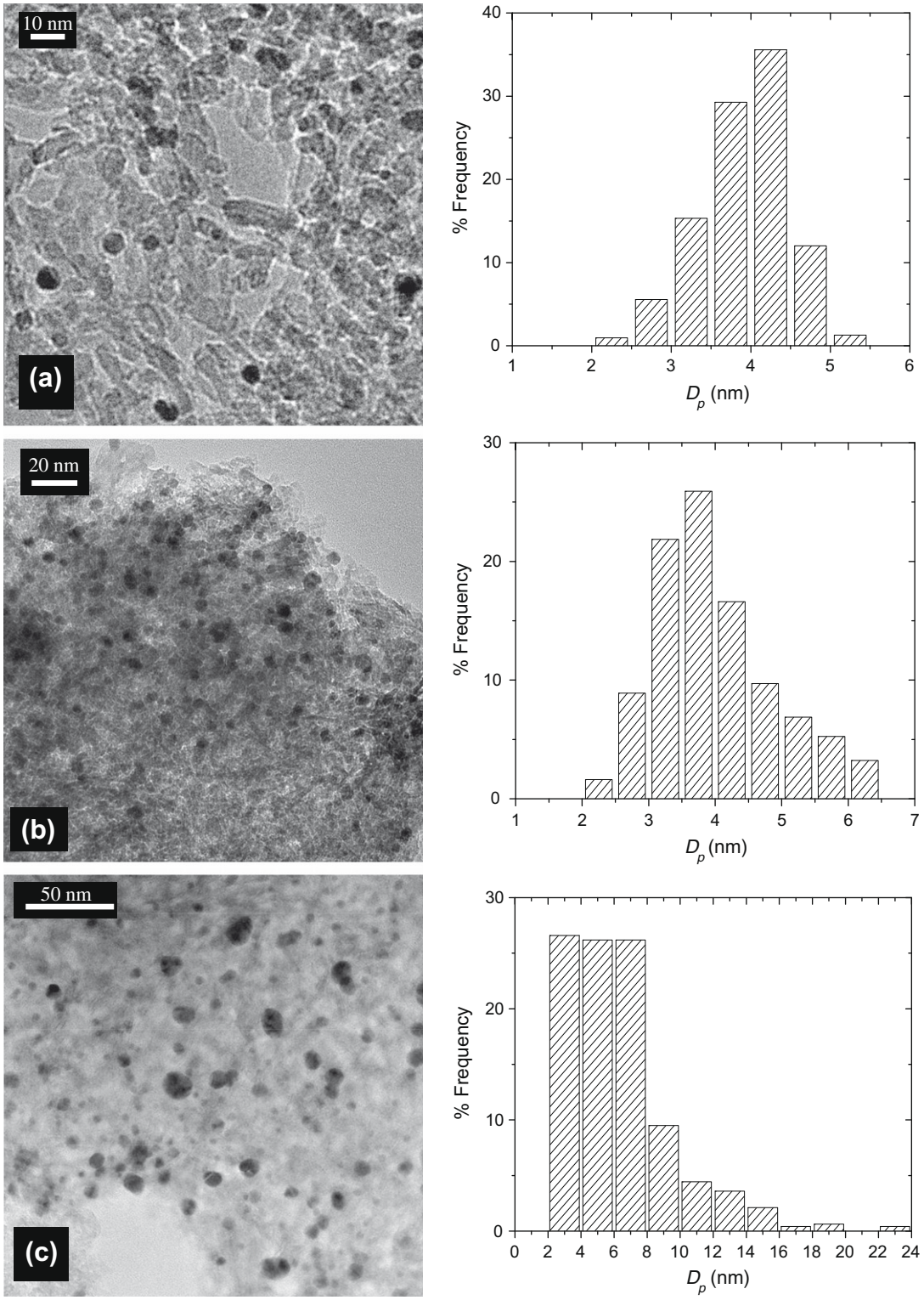

Fig. 3. TEM micrographs and particle size distribution histograms corresponding to the catalysts prepared by immobilization of preformed gold nanoparticles: (a) CAT-DDA, (b) CAT-DDA (w) and (c) CAT-PVP (w).

In the XPS, spectra required for the quantification of the cationic gold species given in Table 3, the deconvolution of the Au *4f* photoelectron region is often fitted using two broad peaks, one representing the Au $4f_{7/2}$ and the other the Au $4f_{5/2}$ line [44–49]. However, the gold nanoparticles formed from gold salt complexes will generate photoelectrons from various gold species present, each of which possessing their specific binding energy. The central peak, Au $4f_{7/2}(2)$, is shifted 0.5–0.8 eV towards lower binding energies with respect to the binding energy of bulk gold at 84.00 eV; see Table 4. This shift is due to the gold atoms in the interior of the nanoparticles. The second component in the measured spectrum, Au $4f_{7/2}(1)$, is assigned to the atoms present at the surface which exhibit a lower coordination than those in the interior. This peak has a lower binding energy (0.6–1.0 eV) when compared with

Table 3
Gold loading (AAS analysis), % weight loss in air (TGA), gold speciation in per cent and elemental composition in atom per cent present at the surface of the investigated catalyst samples (XPS analysis with take-off angle of 45°).

Sample	$[Au]_{total}$ (wt.%)	% wt. loss[a]	Au^0 fraction (%)	Au^+ fraction (%)	Atomic fraction (%)				
					C *1s*	N *1s*	O *1s*	Al *2p*	Au *4f*
WGC	0.8	3[b]	80	20	1.5	0.1	64.8	33.5	0.1
WGC-DDA	0.8	11	80	20	5.9	1.0	59.9	33.1	0.1
Reg. WGC-DDA (2nd use)	0.8	nd[c]	90	10	3.6	0.1	63.6	32.6	0.1
WGC-PVP	0.8	9.4	80	20	0.7	0.2	64.8	34.2	0.1
Reg. WGC-PVP (2nd use)	0.8	nd[c]	70	30	3.1	<0.1	63.2	33.6	0.1
CAT-DDA	0.95	40	97	3	68.5	7.4	16.0	7.6	0.5
Reg. CAT-DDA (2nd use)	0.95	nd[c]	95	5	6.3	0.4	62.2	24.9	0.8
CAT-DDA (w)	1.0	10	74	26	2.4	nd[c]	64.2	33.0	0.5
CAT-PVP (w)	0.82	8	85	15	2.2	0.4	65.1	32.1	0.2

[a] From $T = 696$ K to discard the physisorbed water.
[b] This value can be taken as an approximation of the theoretical mass loss expected in the immobilized gold nanoparticle catalysts after total capping agent removal.
[c] Not determined.

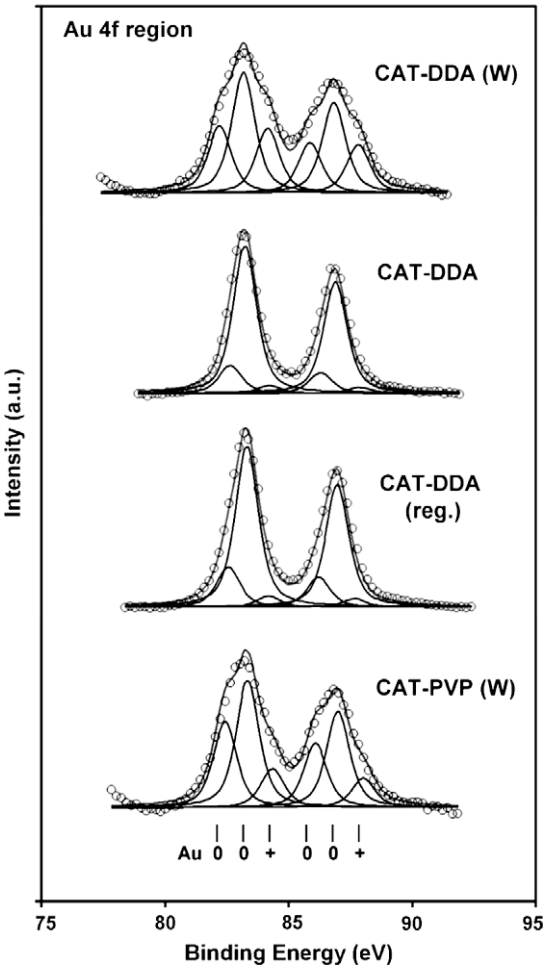

Fig. 4. The deconvolution of the Au *4f* photoelectron region is shown for the supported gold nanoparticles. The catalysts show a three component deconvolution. Two components are assigned to Au^0 species and the third is assigned to Au^+.

Au $4f_{7/2}(2)$. Finally, the third component, Au $4f_{7/2}(3)$, is identified as monovalent cationic gold Au^+. The binding energy of this Au^+ line is 1.0 eV higher than that of the neutral gold Au^0 of Au $4f_{7/2}(2)$, which is in agreement with values reported earlier [34,50].

The approach to deconvolute the Au *4f* region using the measured FWHM is in line with the results of extensive studies [37,51] concluding that the gold and platinum nanoparticles encapsulated act as a metal. Cationic species are formed when

Table 4
The binding energies of the ionic species identified in the Au *4f* photoelectrons for immobilized gold nanoparticles.

Sample	CAT-DDA	Reg. CAT-DDA	CAT-DDA (w)	CAT-PVP (w)	ID
Au $4f_{7/2}$ (1)	82.65	82.55	82.22	82.43	Au^0
Au $4f_{7/2}$ (2)	83.24	83.31	83.18	83.35	Au^0
Au $4f_{7/2}$ (3)	84.21	84.20	84.16	84.36	Au^+
Au $4f_{5/2}$ (1)	86.31	86.21	85.88	86.09	Au^0
Au $4f_{5/2}$ (2)	86.90	86.97	86.84	87.01	Au^0
Au $4f_{5/2}$ (3)	87.87	87.86	87.82	88.02	Au^+

Note: used background is Shirley method.

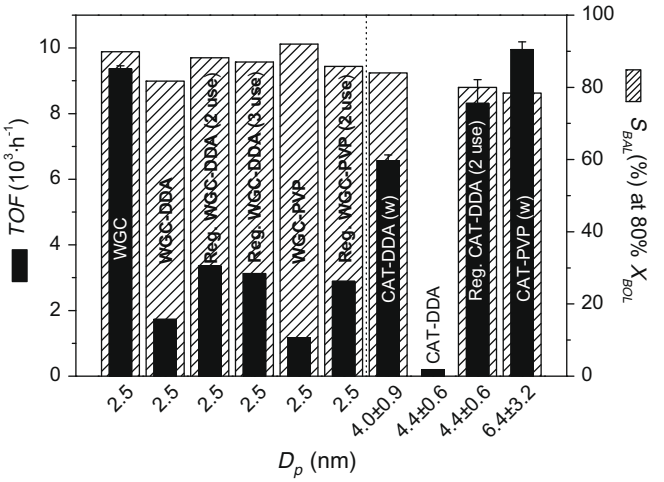

Fig. 5. Initial Turn-Over Frequency (mol benzyl alcohol/mol surface gold/h) and selectivity to benzaldehyde at benzyl alcohol conversion of 80% for different catalyst samples arranged according to increasing gold particle size. Standard reaction conditions: 5.5 mmol BOL, 20 mL toluene, K_2CO_3:BOL = 1:1 mol, 0.2 g catalyst (d_p = 50–70 μm), 353 K, 1 atm air, 100 mL/min (STP) air and 1200 rpm.

the nanoparticle attaches to the alumina support. This effect of the surface active species is shown in Fig. 9 where the specimen CAT-DDA (w) and CAT-PVP (w) exhibit a larger FWHM of the Au *4f* peaks than the freshly prepared CAT-DDA and first time regenerated CAT-DDA. In our model, this broadening is attributed to an increase in both surface species of Au^0 and Au^+ due to an increased interaction with the alumina surface.

The observed binding energy shifts due to a lower coordination of the gold atoms when compared with bulk gold is known as the surface core level shift (SCLS) [52,53]. This initial state effect re-

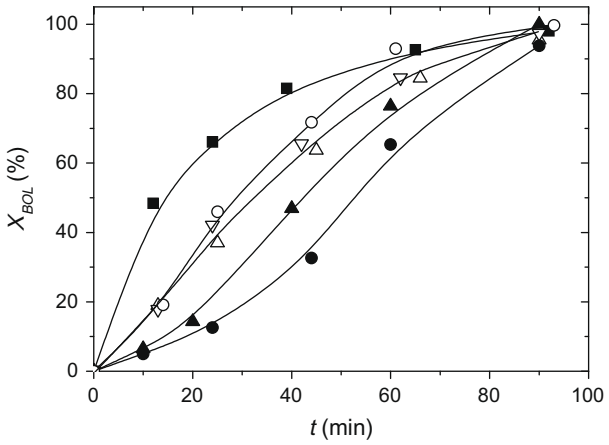

Fig. 6. Conversion as a function of reaction time for the 'as-received' WGC catalyst (0.8 wt.%Au/Al_2O_3) and coated-WGC catalyst exposed to different capping agents (DDA and PVP) during selective oxidation of benzyl alcohol to benzylaldehyde under standard reaction conditions: 5.5 mmol BOL, 20 mL toluene, K_2CO_3:BOL = 1:1 mol, 0.2 g catalyst (d_p = 50–70 μm), 353 K, 1 atm air, 100 mL/min (STP) air and 1200 rpm. Key: ■, WGC; ▲, WGC-DDA; △, Reg. WGC-DDA (2nd use); ▽, Reg. WGC-DDA (3rd use); ●, WGC-PVP; ○, Reg. WGC-PVP (2nd use).

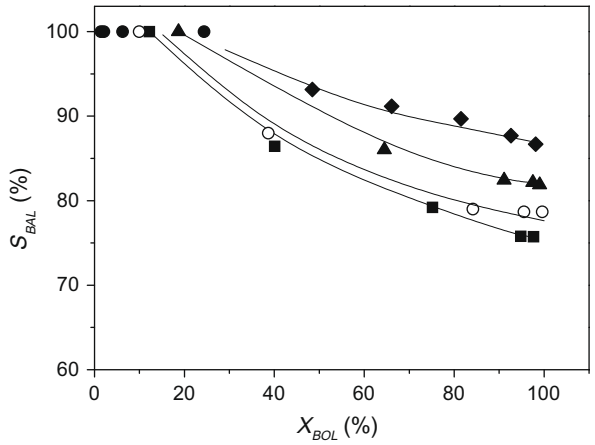

Fig. 7. Selectivity to benzaldehyde (mol benzaldehyde formed per converted mol benzyl alcohol) as a function of benzyl alcohol conversion for different catalysts samples. Standard reaction conditions: 5.5 mmol BOL, 20 mL toluene, K_2CO_3:BOL = 1:1 mol, 0.2 g catalyst (d_p = 50–70 μm), 353 K, 1 atm air, 100 mL/min (STP) air and 1200 rpm.Key: ♦, WGC; ●, CAT-DDA; ○, Reg. CAT-DDA; ▲, CAT-DDA (w); ■, CAT-PVP (w).

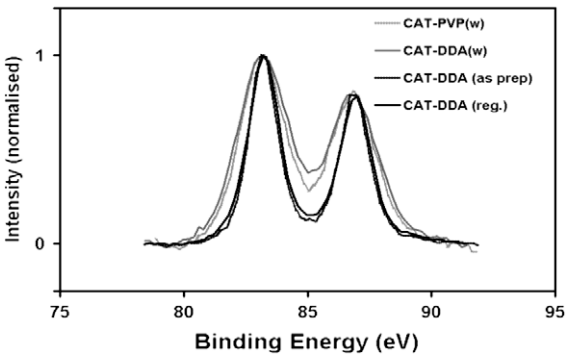

Fig. 9. The normalized intensity of the CAT-DDA and CAT-PVP catalysts reveals the change in linewidth.

sults from the reduction in the binding energy caused by surface atoms lacking neighbouring atoms. This effect is opposed by the electron-core hole generation in XPS in small metallic particles. This final state effect produces a higher binding energy to the photoelectron due to the diminished screening of the core hole. For gold, it results into a reduction of the binding energy.

Han et al. [44] on the other hand explained the negative shift as a result of charge transfer taking place from the γ-Al_2O_3 to the gold nanoparticle, which then becomes negatively charged. In view of the Au^+ species present on the nanoparticle, this is only possible when the electrons transferred have a long enough lifetime thus averting recombination with the cations present.

A special group of catalyst supports concerns reducible oxide materials like CeO_2 as studied by Abad et al. [50] or TiO_2 as studied by Ozkawa et al. [54]. Abad et al. [50] reported values of the Au $4f_{7/2}$ binding energy close to the value of 84.0 eV for bulk gold. This suggests that the mobility of electrons in the support material partially or completely neutralizes or compensates the Au^+ species present. On the other hand, the presence of Au^+ is necessary to explain the catalytic activity of the Au/CeO_2 system. In contrast, Ozkawa et al. [54] showed SCLS to lower binding energy values depending on the coverage of the various TiO_2-supports.

The surface neutral gold species and the monovalent cationic gold add up to constitute 30–50% of the total amount of Au *4f* photoelectrons recorded (*cf.* Table 5). This is consistent with the spherical shape and average diameter of 4 nm of the gold nanoparticles and the inelastic mean free path (IMFP) of 1.3 ± 0.2 nm [55]. In this case the outer edge constitutes about 35% of all gold atoms. The outer species will mainly consist of neutral gold species prone to the surface core level shift and induced Au^+ cations. The analysis

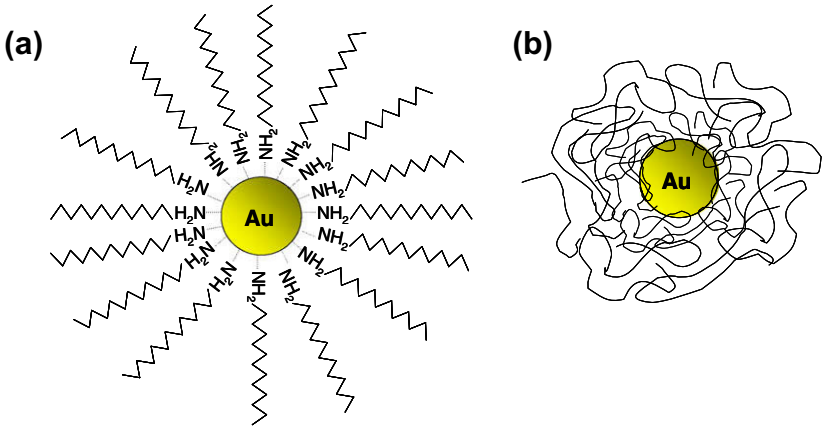

Fig. 8. Schematic illustration of DDA (a) and PVP (b) coated gold nanoparticles.

Table 5
Gold speciation for the immobilized gold nanoparticles given as a percentage of each component.

Sample	CAT-DDA	Reg. CAT-DDA	CAT-DDA (w)	CAT-PVP (w)	ID
Au *4f* (1)	16	19	26	34	Au^0 surface
Au *4f* (2)	82	76	48	51	Au^0 bulk
Au *4f* (3)	3	5	26	15	Au^+
Au *4f* (1 + 3)	19	24	52	49	Au^0 surface + Au^+

depth covers about 70% of the entire volume of the nanoparticle. The interior of the nanoparticle is thought to contain only neutral gold atoms.

The activity of the supported gold catalysts is often attributed to cationic gold species in the catalysts [55–57]. Since the DDA-capped gold nanoparticles in the colloid are not catalytically active whereas, after immobilization, a low at.% of cationic gold species (CAT-DDA in Table 5) appears as long as a slight activity (see Fig. 5 for initial activity, also 24% conversion is achieved after 1.5 h of reaction), it is indeed tempting to attribute the activity for the oxidation of benzyl alcohol to the Au^+ species, in line with the widely accepted reaction mechanism for the selective oxidation of primary alcohols to aldehydes [55–57]:

(1) Metal-alcoholate is first formed in equilibrium with the free alcohol and the cationic species;
(2) The metal-alcoholate reacts to the aldehyde product and the metal-hydride;
(3) Oxygen only regenerates the cationic sites from the metal-hydride.

However, the activity does not correlate well with the present cationic species (Table 3). A better correlation is found with the amount of surface sites exhibiting the surface core level shift or the sum of these with the cationic species (*cf.* Table 5 and Fig. 5). This is better in line with the poisoning experiments of Haider et al. [25] using a thiol-based surfactant which preferably adsorbs at the more extended surface planes of small gold particles and effectively deactivates the catalyst for the benzyl alcohol oxidation.

When the capping agent is present in such excess that the alumina is also covered (see differential thermogravimetric and SDTA profiles in Supplementary material), capping agent molecules can suppress the interaction between the support and the preformed metallic gold nanoparticles resulting in a weak induction of cationic gold species (CAT-DDA of Table 5), located in the interface support–nanoparticle [58,59], as indicated by the small peak widths in Fig. 9. This phenomenon will not only result in a low catalyst activity but also in a low stability. The weak alumina–gold interaction in CAT-DDA is evident by the leaching out of gold. The reaction mixture turned into a reddish colour after reaction though changes in the catalyst content of gold were under the detection limit of the AAS equipment. This did not occur for the catalysts based on the washed nanoparticles.

The support–nanoparticle interaction slightly increased after washing out the capping agent (nitrogen atomic fraction is reduced from 7.4 to 0.4; Table 3), and the activity is re-established in a second use (Fig. 5). The better accessibility of the active sites could explain these results, so the accessibility seems as important for activity as the amount of active sites.

Because the alumina support induces the appearance of the cationic gold and more surface gold atoms after impregnation of the preformed metallic gold nanoparticles; the oxidation of benzyl alcohol is a support-dependent reaction as deduced by comparison of the gold catalytic activity in different studies [25,43,50,60,61].

The results provided by WGC and coated-WGC catalysts (Figs. 5 and 6) confirm that the presence of the capping agents clearly lowers the accessibility of the active sites independently of the concentration of Au^+ species (*cf.* fresh and regenerated CAT-DDA catalysts in Table 2 and Fig. 6). The presence of capping agents may (i) induce diffusion limitations by hindering the approach to the active site due to the formation of a stagnant film, (ii) compete with the benzyl alcohol for the adsorption on the active site, as is known for thiol [25] or (iii) even both. Our results do not allow a further distinction between these two possibilities.

When capping agents participate in the synthesis of the nanoparticles, the use of a capping agent, such as PVP in this study, that promotes polycrystallinity in the particle, can increase the activity to values that compensate the negative effect of a diffusional hindrance. The better accessibility of the active sites by the easier diffusion of the reactants through the porous shell of PVP instead of through a coating layer of the stronger binding DDA (Fig. 8) can positively contribute to the activity (*cf.* CAT-DDA (w) and CAT-PVP (w) in Fig. 5).

In addition, the main difference we observed in the gold particles of CAT-PVP (w) catalyst compared with those of the other catalysts is, apart from their size, related to their crystal structure. PVP promotes the formation of polycrystalline particles which expose more facets and, therefore, more steps/edges. The atoms at the boundaries between multiple crystalline phases are high-energy sites affecting the properties of the nanoparticles such as their reactivity [62,63]. Recent works show that well-defined multiple crystalline nanoparticles of palladium, known as multiple twinned particles, can adsorb a larger quantity of hydrogen [64] or oxygen [65] than their single-crystal analogues. Tang and Ouyang [62] proved, with metal atoms instead of hydrogen or oxygen, that this is a consequence of the faster diffusion rate of the metal atoms along the boundaries of the twinning. Therefore, we propose that the presence of the high-energy atoms in the surface (steps/edges) of the polycrystalline gold particles synthesized in the presence of PVP enhance the diffusion rate of oxygen on the particle to the regenerate the active sites in the catalytic cycle, which may explain the higher activity of CAT-PVP (w) compared with that of WGC and CAT-DDA (w) catalysts with smaller gold particles. Literature indicates an optimum size for supported gold particles in alcohol oxidation [43,66]. The size of the gold particles in the PVP catalyst is around that optimum and can be correlated with the optimum in concentration of surface sites with higher coordination numbers (CN = 8, 9) [67].

This also correlates with the much higher activity of the washed or reused samples of catalysts prepared by impregnation of alumina with the coated gold particles (CAT-DDA (w), CAT-PVP (w) and 2 used CAT-DDA in Fig. 5) than the WGC sample coated with capping agent (WGC-DDA and WGC-PVP). In spite of the smaller gold particles, the activities of the latter are lower.

It is further emphasized that the activities reported here are at least a factor of 10 higher than those reported for TiO_2 and CeO_2 catalysts [43] even when the reaction in our study is conducted at milder conditions (lower temperature and with air instead of using pure oxygen). The reason is unclear but, in the current work, weakly binding capping agents have been used in the preparation of the colloidal nanoparticles in contrast to the phosphorus containing reagent (tetrakis(hydroxymethyl)phosphonium chloride)

used in Ref. [43]. Hutchings et al. extensively studied the solvent-free benzyl alcohol oxidation over supported Au and Au–Pd nanocrystals [68–71]. However, their applied conditions are harsher than those used here, temperatures between 100 and 160 °C and pressures between 2 and 10 bar O_2. The TOFs of the pure gold catalysts are still lower than in the current study [68], although the addition of Pd increases the activity, but also lowers the selectivity [69]. Toluene was an important by-product observed. Due to its use as solvent in the current study, this formation could not be here quantified, but considering their work at the mildest conditions [68] this compound is hardly expected.

Catalytic selectivity depends on factors such as the oxide–metal interface, particle size, surface structure and selective blocking of surface sites [72]. There is always a major dominating factor for each reactant-catalyst system. By experimentation with catalysts prepared using the nanotechnology methods, an independent analysis of the factors has become available and also the elucidation of the dominating one for a particular catalytic reaction [25,73]. In the oxidation of cinnamyl alcohol to cinnalmaldehyde on Au/TiO_2 catalysts, the selectivity is independent of gold particle size [50], like for the oxidation of benzyl alcohol on Au/TiO_2 and Au/CeO_2 catalysts [43]. All these reactions were performed in liquid phase. In our study, this selectivity seems to increase with decreasing gold particle size, independent of the presence of a capping agent and the twinning defects in the gold particles, at least at 353 K (Fig. 5). The support may dominate this effect as TiO_2 gave a higher selectivity than CeO_2 [43]. The use of a non-polar solvent can contribute to the high selectivity values [43,60]. We observed 100% selectivities up to 20% conversion, after which the selectivity gradually decreased (Fig. 7), as is expected in a consecutive reaction scheme, to 75–90% values. The larger particles clearly exhibited a lower selectivity than the smaller gold particles, irrespective of their origin.

5. Conclusions

Gold on alumina catalysts prepared via a colloidal route using nitrogen-based capping agents DDA and PVP have a high activity in the liquid phase oxidation of benzyl alcohol. Supported gold particles with the same size, shape, crystallinity and similar number of active sites show significantly higher initial TOF values in the absence of capping agents. The capping agents may induce diffusion limitations by hindering the approach to the active site due to the formation of a stagnant film, may compete with the reactant for the adsorption on the active site or even both. We could not distinguish unequivocally between these phenomena.

The gold nanoparticles in colloidal solution with capping agent are metallic and show no activity in selective oxidation reactions. When brought on a support, three different gold species, *viz.* surface and interior metallic gold and monovalent gold (Au^+) are identified from photoelectron spectra. The interaction of support–nanoparticle induces the presence of cationic gold and increased surface gold atoms. Their concentration correlates with the catalytic activity, even if capping agent is present, and suggests that active surface sites have higher coordination numbers (CN = ~8, 9).

Capping agent PVP that weakly adsorb on the particle creates a porous layer around the particle during synthesis and promotes polycrystallinity, resulting in nanoparticles with twinning defects and with enhanced activity even compensating the negative effect of diffusional hindrance. The larger PVP-based polycrystalline nanoparticles are more catalytically active than the smaller DDA-based single-crystal nanoparticles. On the contrary, selectivity at high conversions is dominated by the gold particle size on alumina and increases with the decreasing size independent of the presence of capping agents and twinning defects.

Acknowledgments

Financial support was provided by Delft Centre for Sustainable Industrial Processes (DC-SIP). Patricia J. Kooyman and Ugo Lafont of Delft University of Technology are gratefully thanked for fruitful TEM discussions. The authors also thank Ángel Berenguer-Murcia and the World Gold Council for the kind supply of the PVP-coated gold sol and reference catalyst (BC17), respectively.

Appendix A. Supplementary material

Supplementary data associated with this article can be found, in the online version, at doi:10.1016/j.jcat.2010.02.013.

References

[1] M.C. Daniel, D. Astruc, Chem. Rev. 104 (2004) 293.
[2] J. Shan, H. Tenhu, Chem. Commun. (2007) 4580.
[3] J. Park, J. Joo, S.G. Kwon, Y. Jang, T. Hyeon, Angew. Chem. Int. Ed. 46 (2007) 4630.
[4] B. Zhou, S. Hermans, G.A. Somorjai, Nanotechnology in Catalysis, vol. 1, Springer, New York, 2004. Chapter 5.
[5] Y. Sun, B. Mayers, T. Herricks, Y. Xia, Nano Lett. 3 (2003) 955.
[6] C.J. Murphy, Science 298 (2002) 2139.
[7] K.M. Bratlie, H. Lee, K. Komvopoulos, P. Yang, G.A. Somorjai, Nano Lett. 7 (2007) 3097.
[8] A.R. Tao, S. Habas, P. Yang, Small 4 (2008) 310.
[9] G.H. Zhang, W.L. Guo, X.K. Wang, Mater. Res. Innovat. 11 (2007) 201.
[10] S. Tsubota, T. Nakamura, K. Tanaka, M. Haruta, Catal. Lett. 56 (1998) 131.
[11] H. Lang, R.A. May, B.L. Iversen, B.D. Chandler, J. Am. Chem. Soc. 125 (2003) 14832.
[12] G. Martra, L. Prati, C. Manfredotti, S. Biella, M. Rossi, S. Coluccia, J. Phys. Chem. B 107 (2003) 5453.
[13] L.D. Menard, F. Xu, R.G. Unzo, J.C. Yang, J. Catal. 243 (2006) 64.
[14] H. Lee, S.E. Habas, S. Kweskin, D. Butcher, G.A. Somorjai, P. Yang, Angew. Chem. Int. Ed. 45 (2006) 7824.
[15] L. Prati, G. Martra, Gold Bull. 32 (1999) 96.
[16] Y. Li, M.A. El-Sayed, J. Phys. Chem. B 105 (2001) 8938.
[17] R.M. Crooks, M. Zhao, L. Sun, V. Chechik, L.K. Yeung, Acc. Chem. Res. 34 (2001) 181.
[18] S. Biella, F. Porta, L. Prati, M. Rossi, Catal. Lett. 90 (2003) 23.
[19] N. Dimitratos, A. Villa, C.L. Bianchi, L. Prati, M. Makkee, Appl. Catal. A Gen. 311 (2006) 185.
[20] R. Raja, V.B. Golovko, J.M. Thomas, A. Berenguer-Murcia, W. Zhou, S. Xie, B.F. Johnson, Chem. Commun. (2005) 2026.
[21] S. Domínguez-Domínguez, A. Berenguer-Murcia, D. Cazorla-Amorós, A. Linares-Solano, J. Catal. 243 (2006) 74.
[22] Z. Zhang, F. Wang, F. Chen, G. Shi, Mater. Lett. 60 (2006) 1039.
[23] D.S. Sidhaye, B.L.V. Prasad, Chem. Phys. Lett. 454 (2008) 345.
[24] A. Quintanilla, V.C.L. Butselaar-Orthlieb, C. Kwakernaak, W.G. Sloof, M.T. Kreutzer, F. Kapteijn, Towards an integrated approach in innovation and development, in: Proc. WCOC6, 5–10 July 2009, Lille, France, p. 146.
[25] P. Haider, A. Urakawa, E. Schmidt, A. Baiker, J. Mol. Catal. A.: Chem. 305 (2009) 161.
[26] Y. Chen, X. Wang, Mater. Lett. 62 (2008) 2215.
[27] F. Fievet, J.P. Lagier, B. Blin, B. Beaudoin, M. Figlarz, Solid State Ion. 32 (1989) 198.
[28] P. Lu, T. Teranishi, K. Asakura, M. Miyake, N. Toshima, J. Phys. Chem. B 103 (1999) 9673.
[29] Y. Sun, Y. Xian, Adv. Mater. 14 (2002) 833.
[30] B. Wiley, Y. Sun, B. Mayers, Y. Xia, Chem. Eur. J. 11 (2005) 454.
[31] B. Lim, M. Jiang, J. Tao, P.H.C. Camargo, Y. Zhu, Y. Xia, Adv. Funct. Mater. 19 (2009) 189.
[32] ASTM Standard E902-88, Surf. Interface Anal. 17 (1991) 889.
[33] P. Swift, Surf. Interface Anal. 4 (1982) 47.
[34] NIST X-ray Photoelectron Database, Web Version 3.5. <http://srdata.nist.gov/xps/Default.aspx>.
[35] J. Chastain, Handbook of X-ray Photoelectron Spectroscopy, Perkin–Elmer Corporation, Eden Prairie, USA, 1992.
[36] J. Chen, Q. Zhang, Y. Wang, H. Wan, Adv. Synth. Catal. 350 (2008) 453.
[37] D.V. Leff, L. Brandt, J.R. Heath, Langmuir 12 (1996) 4723.
[38] Z. Zhang, B. Zhao, L. Hu, J. Solid State Chem. 121 (1996) 105.
[39] F. Bonet, K. Teikaia-Elhsissen, K. Vijaya Sarathy, Bull. Mater. Sci. 23 (2000) 165.
[40] M. Comotti, C. Pina, R. Matarrese, M. Rossi, Angew. Chem. Int. Ed. 43 (2004) 5812.
[41] P.G.N. Mertens, I.F. Vankelecom, P.A. Jacobs, D.E. De Vos, Gold Bull. 38 (2005) 157.
[42] F. Porta, L. Prati, M. Rossi, G. Scari, J. Catal. 211 (2002) 464.
[43] P. Haider, B. Kimmerle, F. Krumeich, W. Kleist, J. Grunwaldt, A. Baiker, Catal. Lett. 125 (2008) 169.

[44] Y.F. Han, Z. Zhong, K. Ramesh, F. Chen, F. Chen, L. Chen, J. Phys. Chem. C 111 (2007) 3163.
[45] A.M. Venezia, V. La Parola, B. Pawelec, J.L.G. Fierro, Appl. Catal. A Gen. 264 (2004) 43.
[46] B. Paweleca, A.M. Veneziab, V. La Parola, E. Cano-Serranoa, J.M. Campos-Martina, J.L.G. Fierro, Appl. Surf. Sci. 242 (2005) 380.
[47] Z. Suo, C. Ma, M. Jin, T. He, L. An, Catal. Commun. 9 (2008) 2187.
[48] S. Schimpf, M. Lucas, C. Mohra, U. Rodemerck, A. Brückner, J. Radnik, H. Hofmeister, P. Claus, Catal. Today 72 (2002) 63.
[49] T. Herranz, X. Deng, A. Cabot, P. Alivisatos, Z. Liu, G. Soler-Illia, M. Salmeron, Catal. Today 143 (2009) 158.
[50] A. Abad, P. Concepción, A. Corma, H. García, Angew. Chem. Int. Ed. 44 (2005) 4066.
[51] Y. Borodko, S.E. Habas, M. Koebel, P. Yang, H. Frei, G.A. Somorjai, J. Phys. Chem. B 110 (2006) 23052.
[52] A. Zwijnenburg, A. Goossens, W.G. Sloof, M.W.J. Crajé, A.M. van der Kraan, L.J. de Jongh, M. Makkee, J.A. Moulijn, J. Phys. Chem. B 106 (2002) 9853.
[53] N.R. Shamsutdinov, W.G. Sloof, A.J. Böttger, J. Appl. Phys. 98 (2005) 014908.
[54] T. Okazawa, M. Kohyama, Y. Kido, Surf. Sci. 600 (2006) 4430.
[55] T. Mallat, A. Baiker, Chem. Rev. 104 (2004) 3037.
[56] A. Abad, A. Corma, H. Garcia, Chem. Eur. J. 14 (2008) 212.
[57] G. Brink, I.W.C.E. Arends, R.A. Sheldon, Science 287 (2000) 1636.
[58] J.C. Fierro-Gonzalez, B.C. Gates, Chem. Soc. Rev. 37 (2008) 2127.
[59] G.C. Bond, C. Louis, D.T. Thompson, Catalysis by Gold, Imperial College Press, London, 2006, p. 195.
[60] J. Hu, L. Chen, K. Zhu, A. Suchopar, R. Richards, Catal. Today , 122 (2007) , p. 277.
[61] F. Su, Y. Liu, L. Wang, Y. Cao, H. He, K. Fan, Angew. Chem. Int. Ed. 47 (2008) 334.
[62] Y. Tang, M. Ouyang, Nat. Mater. 6 (2007) 754.
[63] G.V. Hartland, Nat. Mater. 6 (2007) 716.
[64] F. Calvo, A. Carré, Nanotechnology 17 (2006) 1292.
[65] Y. Xiong, J.M. McLellan, Y. Yin, Y. Xia, Angew. Chem. Int. Ed. 46 (2007) 790.
[66] K. Sun, S. Luo, N. Xu, B. Xu, Catal. Lett. 124 (2008) 238.
[67] T.V.W. Janssens, B.S. Clausen, B. Hvolbæk, H. Falsig, C.H. Christensen, T. Bligaard, J.K. Nørskov, Top. Catal. 44 (2007) 15.
[68] D.I. Enache, D.W. Knight, G.J. Hutchings, Catal. Lett. 103 (2005) 43.
[69] D.I. Enache, D. Barker, J.K. Edwards, S.H. Taylor, D.W. Knight, A.F. Carley, G.J. Hutchings, Catal. Today 122 (2007) 407.
[70] J.A. Lopez-Sanchez, N. Dimitratos, P. Miedziak, E. Ntainjua, J.K. Edwards, D. Morgan, A.F. Carley, R. Tiruvalam, C.J. Kiely, G.J. Hutchings, Phys. Chem. Chem. Phys. 10 (2008) 1921.
[71] N. Dimitratos, J.A. Lopez-Sanchez, D. Morgan, A.F. Carley, R. Tiruvalam, C.J. Kiely, D. Bethell, G.J. Hutchings, Phys. Chem. Chem. Phys. 11 (2009) 5142.
[72] G.A. Somorjai, R.M. Rioux, Catal. Today 100 (2005) 201.
[73] G.A. Somorjai, F. Tao, J.Y. Park, Top. Catal. 47 (2008) 1.